

Large-area synthesis of continuous two-dimensional $\text{MoTe}_x\text{Se}_{2-x}$ alloy films by chemical vapor deposition

Shudong Zhao¹, Meilin Lu¹, Shasha Xue¹, Lei Tao², Yu Sui¹, Yang Wang³

¹ Department of Physics, Harbin Institute of Technology, Harbin 150001, People's Republic of China.

² Laboratory for Space Environment and Physical Sciences, Harbin Institute of Technology, Harbin 150001, People's Republic of China

³ Academy of Fundamental and Interdisciplinary Sciences, Harbin Institute of Technology, Harbin 150001, People's Republic of China.

‡ Shudong Zhao and Meilin Lu contributed equally to this work

E-mail: taolei@hit.edu.cn (Lei Tao); suiyu@hit.edu.cn (Yu Sui); yangwang@hit.edu.cn (Yang Wang)

Abstract

Great achievements have been made in alloying of two-dimensional (2D) semiconducting transition metal dichalcogenides (TMDs), which can allow tunable band gaps for practical applications in optoelectronic devices. However, telluride-based TMDs alloys were less studied due to the difficulties of sample synthesis. Here, in this work we report the large-area synthesis of 2D $\text{MoTe}_x\text{Se}_{2-x}$ alloy films with controllable Te composition by a modified alkali metal halides assisted chemical vapor deposition method. The as-prepared films have millimeter-scale transverse size. Raman spectra experiments combining calculated Raman spectra and vibrational images obtained by density functional theory (DFT) confirmed the 2H-phase of the $\text{MoTe}_x\text{Se}_{2-x}$ alloys. The A_{1g} mode of MoSe_2 shows a significant downshift accompanied by asymmetric broadening to lower wavenumber with increasing value of x , while E^{1}_{2g} mode seems unchanged, which were well explained by a phonon confinement model. Our work provides a simple method to synthesize large-scale 2H phase Te-based 2D TMDs alloys for their further applications.

Keyword: TMDs alloys, large-area, CVD, Raman, DFT;

1. Introduction

Two dimensional (2D) semiconducting transition metal dichalcogenides (TMDs) have shown great potential applications in the area of electronics¹, optoelectronics² and electrochemistry³. Alloying is a powerful method to tailor the properties of TMDs, which can tune their band gaps continuously between the two ends of one series as a function of chemical composition⁴. For instance, the direct-band gap of monolayer $\text{MoS}_x\text{Se}_{2-x}$ can be tuned between the values of single-layer MoS_2 (~ 1.9 eV) and MoSe_2 (~ 1.5 eV)⁵⁻⁸. In general there are two kinds of alloying in TMDs, one is at transition metal sites and another one is at chalcogenide site. Previously, several series of 2D semiconducting TMDs alloys have been obtained by exfoliation or chemical vapor deposition (CVD) methods, such as $\text{Mo}_{1-x}\text{W}_x\text{S}_2$ ^{9, 10}, $\text{Mo}_{1-x}\text{W}_x\text{Se}_2$ ¹¹, $\text{WS}_{2(1-x)}\text{Se}_{2x}$ ^{12, 13}. These series of TMDs alloys usually have 2H structure, realizing the tunable direct-band gap from 1.5 eV to 2.1 eV.

It is difficult to prepared 2H-phase Te-based TMDs or their alloys, especially using CVD, because it always undergoes a phase transition from 2H to 1T' at cooling stage, thus resulting in the metallic or semi-metallic samples¹⁴⁻¹⁶. Amey Apte et al. reported a facile single-step CVD synthesis of 2H $\text{MoTe}_x\text{Se}_{2-x}$ monolayers¹⁷. However, the surface of as-grown nanosheets is not uniform and the size is small, limiting their applications in practice. Thus, a special method is pressingly needed to obtain 2D TMDs alloys at large scale.

Recently, molten-salt-assisted CVD has been successfully used to synthesize large-area and a wide variety of TMDs and their alloys^{18, 19}. Here, we report a modified molten-salt-assisted CVD method to synthesize large area continuous 2D $\text{MoTe}_x\text{Se}_{2-x}$ films. Through tuning the heating temperature of Te powders, we prepared two kinds of $\text{MoTe}_x\text{Se}_{2-x}$ films with different Te alloying concentrations. Combining Raman scattering experiments and density functional theory calculation results we confirmed that the as-grown $\text{MoTe}_x\text{Se}_{2-x}$ films are 2H phase and the corresponding compositions of Te are about 0.11 and 0.25 respectively. The composition dependent behaviors of Raman peaks were well explained by a phonon confinement model. Our work provides a fundamental research for the applications of TMDs alloys.

2. Methods

2.1. Sample preparation

Large area continuous $\text{MoTe}_x\text{Se}_{2-x}$ films were synthesized in a home-built three-temperature-zone (a single-zone low-temperature furnace and a two-zone high temperature furnace) CVD system. The low-temperature furnace at upstream was used to heat Se powders (350 °C) and the high temperature furnace at downstream was used to heat Te powders (550 °C or 580 °C) and Mo precursors and substrates. The same

weight (2 g) of Se and Te powders was used. 20 mg of MoO₃ powders and NaCl powders (2:1) were mixed by grinding together in a mortar and then were pressed into a disc at 10 MPa as the Mo precursors. The disc was placed on a quartz sheet and a piece of SiO₂/Si substrate was placed next to the disc at downstream. The pressure in the 2 inch furnace tube was firstly pumped down to 10 mTorr, then kept at 100 Torr with 55 sccm Ar and 3 sccm H₂ as the carrier gas. The growth temperature was 750 °C and time was 5 min. Then the furnace cooled down to room temperature gradually.

2.2. Raman characterization

Raman measurements were performed under atmospheric environment in a Renishaw inVia Raman microscope equipped with a 532 nm laser. The system was firstly calibrated with the strongest Raman peak of silicon at 520 cm⁻¹ before measurements.

2.3. Density functional theory calculation

Raman spectra and vibrational modes of monolayer MoTe_xSe_{2-x} at two composition ($x = 0.11$ and $x = 0.25$) were calculated by density functional theory (DFT). The 3×3 supercell with one Te atom corresponds to $x = 0.11$, and the 2×2 supercell with one Te atom corresponds to $x = 0.25$. Vacuum spacing in the out-of-plane direction is set to be more than 18 Å to avoid spurious interaction. Structure and phonon properties are calculated by Vienna ab initio simulation package (VASP) using the projector-augmented wave (PAW) methods and Perdew-Burke-Ernzerhof (PBE) functional with D3 correction (DFT-D3). The energy cutoff was set as 400 eV and residual forces for ion iteration as 10⁻⁴ eV/Å. The Γ -centered Monkhorst-Pack (MP) k-points were set as 12×12×1 and 16×16×1 for $x = 0.11$ and $x = 0.25$ respectively. After the structural relaxations, the normal vibration modes are calculated within frozen phonon approximation. Giving these vibration mode, Raman intensities are obtained based on the calculation of the derivatives of the dielectric tensors with respect to phonon vibration using script “vasp_raman.py”. This is a Raman off-resonant activity calculator using VASP as a back end. Lorentz broadening of the modes’ intensities yielded the Raman spectrum.

3. Results and discussion

3.1. Synthesis of 2D MoSe_{2(1-x)}Te_x film

Figure 1a shows the schematic diagram of our CVD process. We used the molten-salt-assisted CVD methods reported previously to synthesize 2D MoSe₂ nanosheets and MoTe_xSe_{2-x} alloys¹⁹. At the pre-exploration stage of our experiments, the mixed MoO₃ and NaCl powders were used to grow MoSe₂ as previous works did (see Figure S1a). Contrary to our expectation, the size of as-prepared MoSe₂ turned out to be small (see Figure S1b). It seems to be ascribed to insufficient contact between MoO₃ and NaCl.

As we can see in Figure S1c, the mixed powders just partially reacted with Se through a short growth time (5 min). In order to make the MoO₃ and NaCl to contact sufficiently, we pressed the mixed powders to a disc as seen in Figure S1d. By this means, the full reaction of MoO₃, NaCl and Se was realized, resulting in large-area growth of MoSe₂ films (see Figure S1e and S1f).

Then this modified molten-salt-assisted method was used to synthesize 2D MoSe_{2-x}Te_x alloy films. In a recent work, it has been demonstrated that large amount of Te alloying in WSe_{2(1-x)}Te_{2x} (more than 0.5) leads to a phase transition from 2H to 1T'²⁰. To avoid this phenomena, the heating temperature of Te powders was set at a lower point (550 °C). Figure 1(b) and 1(c) shows the optical images of as-prepared MoSe_{2-x}Te_x continuous film at different magnifications, indicating the large area and its smooth surface. The scratch at the central area was made by sharp tweezers for the characterization of its thickness. As seen in figure 1(d), the height image and profile of atomic force microscope (AFM) confirm that the MoTe_xSe_{2-x} film is a bilayer and has a relatively smooth surface except a little amount of nanoparticles on it.

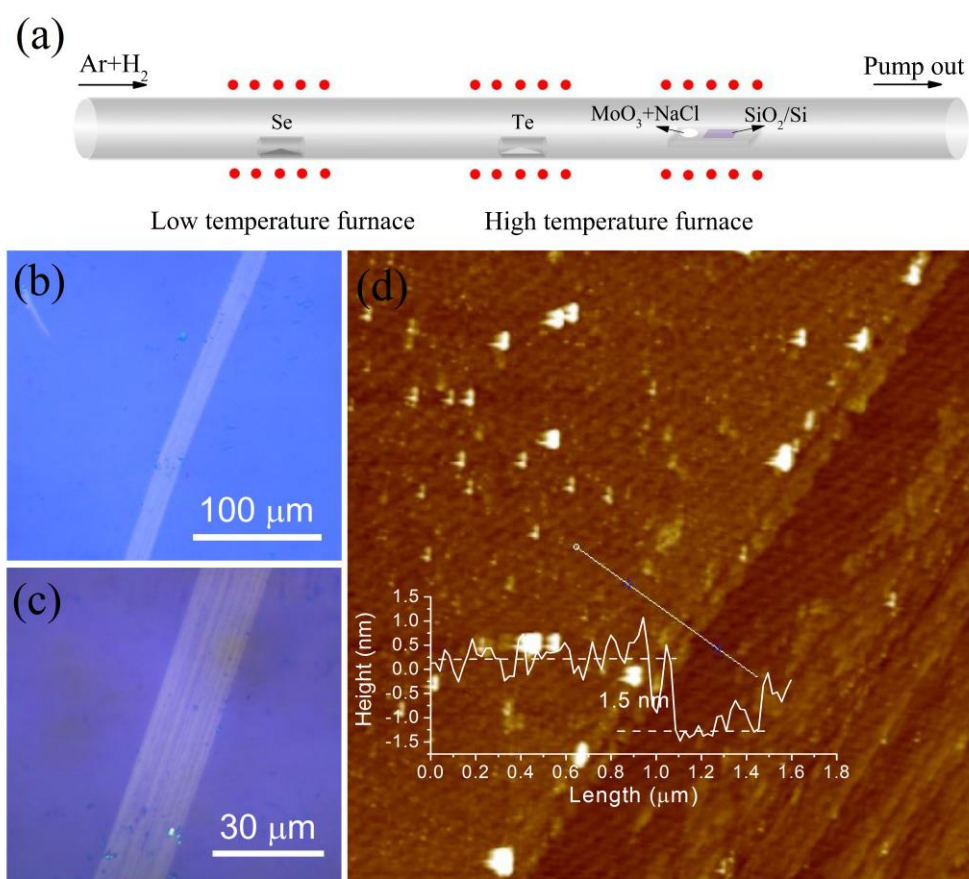


Figure 1 (a) Schematic diagram of the CVD system. (b) Optical image of as-prepared MoTe_xSe_{2-x} continuous film under 10x objective. (c) under 40x objective. (d) AFM height image and profile of the corresponding MoTe_xSe_{2-x} film.

3.2. Raman characterization and the behaviors of Raman modes

The composition of Te in MoTe_xSe_{2-x} alloys can be easily tailored by modifying the

heating temperature of Te powders to 580 °C. Figure 2 gives the Raman spectra of the as-grown MoSe₂ and MoTe_xSe_{2-x} alloys at two different Te heating temperatures. The Raman spectrum of pristine MoSe₂ shows one sharp peak at 240 cm⁻¹ corresponding to A_{1g} mode, and a weak peak at 286 cm⁻¹ corresponding to E¹_{2g} mode. With increasing composition *x*, the A_{1g} peak shows a significant downshift (from 240 cm⁻¹ to 230 cm⁻¹) in MoTe_xSe_{2-x} alloys, as well as the asymmetric broadening to lower frequency. However, the frequency of E¹_{2g} mode seems unchanged and just shows a peak broadening.

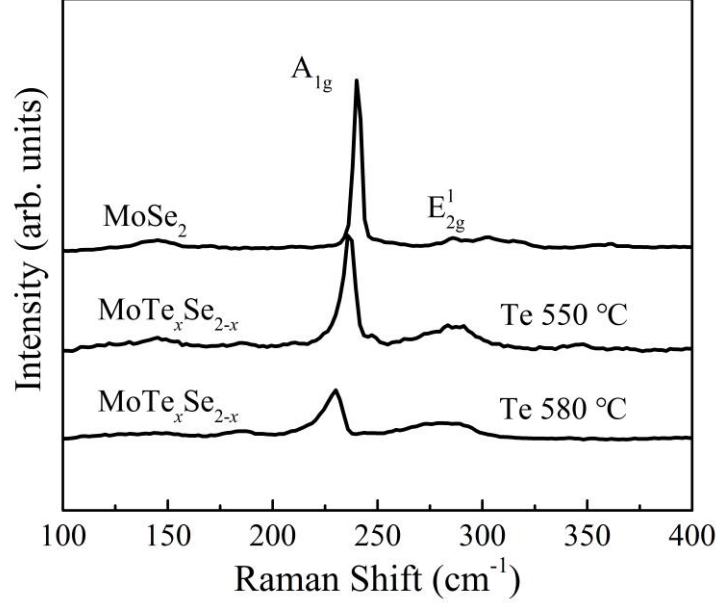


Figure 2 Raman spectra of as-grown MoSe₂ and MoSe_{2-x}Te_x alloys

Similar behaviors of A_{1g} mode and E¹_{2g} mode were also observed both in MoS_xSe_{2-x} alloy series when $x \leq 1^5$ and in Se deficient MoSe_{2-x} nanosheets²¹. The evolution of intrinsic Raman bands with increasing defect density can be explained by a phonon confinement model. After introducing defects in a crystalline material, the translational symmetry of the system is broken and the phonons are confined in a small region, resulting in relaxation of the fundamental Raman selection rule²². As to 2D system, the phonon confinement model can be described as²³:

$$I(\omega) = \int \frac{\exp(-q^2 L_D / 2\alpha)}{(\omega - \omega(q))^2 + (\Gamma_0 / 2)^2} 2\pi q dq \quad (1)$$

where L_D is the average distance of defects or the domain size, corresponding to the density of defects and $\omega(q)$ is the phonon dispersion of 2D MoSe₂.

The phonon dispersion of monolayer MoSe₂ calculated by DFT is shown in figure 3(a). The dispersion curves of both two branches of E¹_{2g} mode are relatively flat throughout the Brillouin zone. While, the frequency of A_{1g} mode shows downshift along both Γ -K and Γ -M directions. The evolutions of positions of E¹_{2g} and A_{1g} peaks in Raman spectra agree very well with their phonon dispersion. Because the E¹_{2g} peak

is weak and its peak position changes little, we just simulated the Raman spectra of A_{1g} mode using equation (1). The simulation results are illustrated in figure 3(b) and 3(c), the value of α we used is 0.001. As can be seen, the simulated curves fit well with the experimental data.

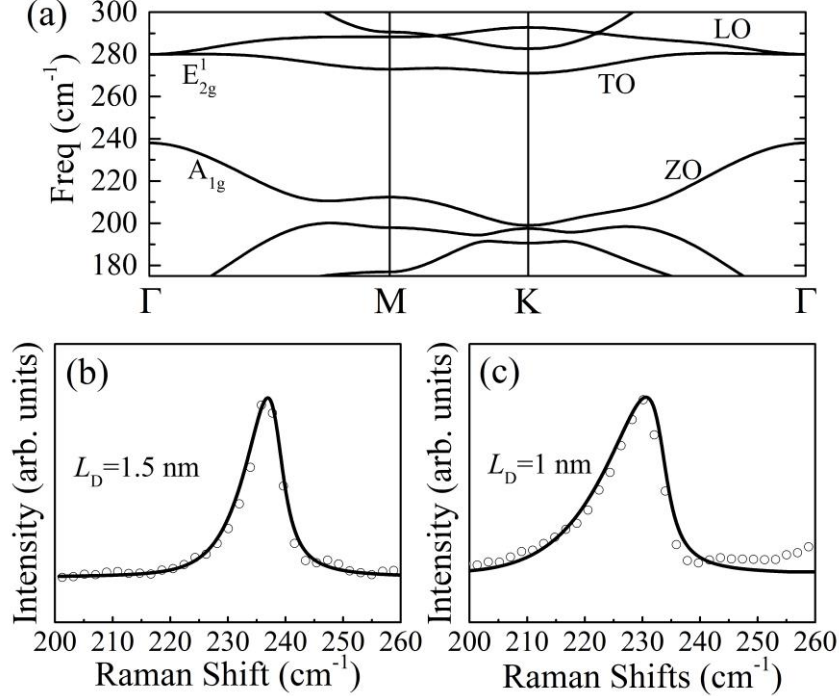


Figure 3 (a) Phonon dispersion of monolayer MoSe₂. (b) and (c) Simulated Raman spectra of 2D MoTe_xSe_{2-x} films, black line is the simulation result and black circle is the experimental data.

In addition, we also used DFT method calculated the vibrational modes and Raman spectra of 2H phase MoTe_xSe_{2-x} at two Te alloying concentrations, 0, 0.11 and 0.25 respectively (see details in Methods and figure S2). As illustrated in figure 4, when $x = 0$, it is MoSe₂ and the modes at 238 cm⁻¹ and 280 cm⁻¹ represent A_{1g} and E_{2g}^1 modes respectively. Se atoms at top and bottom layers vibrate out phase along vertical direction while Mo atoms are static in A_{1g} mode. As in E_{2g}^1 mode, all Se atoms vibrate in phase as well as Mo atoms along armchair or zigzag directions (LO or TO), but Se and Mo atoms vibrate out phase. These are typical vibrational images of optical phonons of monolayer MoSe₂. When $x = 0.11$, there are also two mode at 235 cm⁻¹ and at 280 cm⁻¹. In general, the vibrational image of mode at 235 cm⁻¹ is quite similar with A_{1g} mode in MoSe₂. That is atoms in top chalcogenide layer still vibrate in phase along vertical direction and out phase with the atoms in bottom layer, so it can be assigned to A_{1g} mode. As to the mode at 280 cm⁻¹, all chalcogenide atoms vibrate in phase and out phase with Mo atoms in xy plane, so it can be assigned to E_{2g}^1 mode. The same phenomena can be observed when $x = 0.25$, but just the A_{1g} mode moves to 230 cm⁻¹ and the frequency of E_{2g}^1 mode is unchanged. The evolution of peak frequency shifts of the first-order Raman modes obtained by DFT calculation shows high agreement with the experimental results. And surprisingly, the calculated peak positions of

$\text{MoTe}_x\text{Se}_{2-x}$ are just corresponding to the positions in the experimental Raman spectra, which can be an indirect characterization of the Te alloying concentrations in $\text{MoTe}_x\text{Se}_{2-x}$ films.

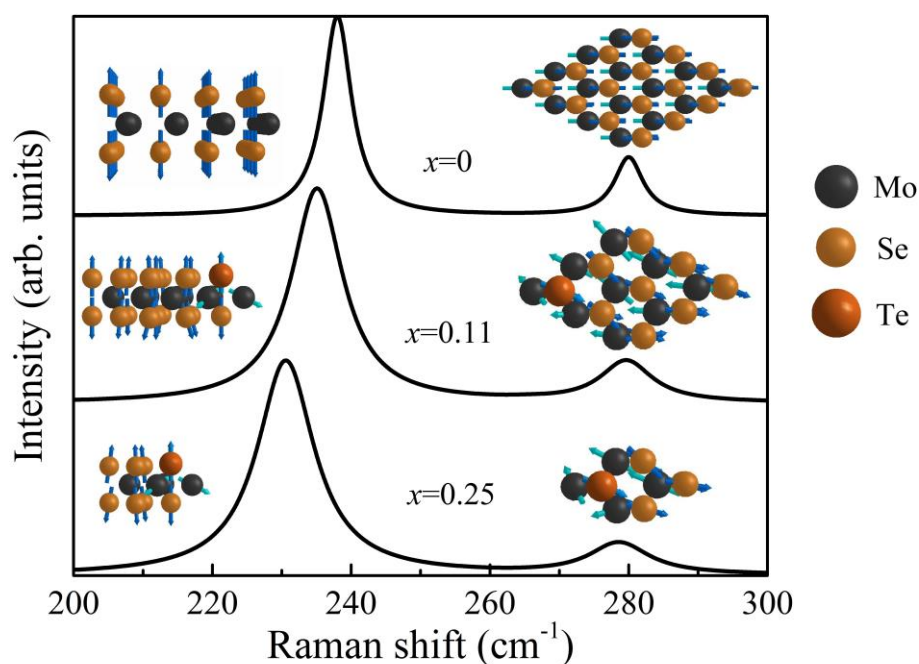


Figure 4 Calculated Raman spectra and atomic vibrational images of $\text{MoTe}_x\text{Se}_{2-x}$ films at three different compositions.

4. Conclusions

In summary, we have synthesized large-area continuous 2H phase $\text{MoSe}_{2-x}\text{Te}_x$ films, and tailored the Te composition through modifying the heating temperature of Te powders independently in a three-temperature-zone CVD process. The evolution of peak position shifts and linewidths of the A_{1g} mode and E_{2g}^1 mode is well explained with the phonon confinement model using the phonon dispersion of MoSe_2 calculated by DFT. On the other hand, the Raman spectra and atomic vibrational images of 2D $\text{MoSe}_{2-x}\text{Te}_x$ obtained by DFT calculation give an additional view of the behaviors of the first-order optical phonons with increasing Te compositions, which also agree very well with the experimental data. This work provides a simple method to synthesize large-scale 2D $\text{MoTe}_x\text{Se}_{2-x}$ alloy series and gives a fundamental study of their Raman scattering properties.

Supporting information

Supporting information is available on line or from author.

Acknowledgements

This study was financially supported by the National Natural Science Foundation of China (No. 11304060) and the Foundation of Harbin Institute of Technology for the

Incubation Program of the development of basic research outstanding talents (No. 01509321) and the China Postdoctoral Science Foundation.

References

1. Radisavljevic, B.; Radenovic, A.; Brivio, J.; Giacometti, i. V.; Kis, A. J. N. n., Single-layer MoS₂ transistors. **2011**, *6* (3), 147.
2. Ponomarev, E.; Gutiérrez-Lezama, I.; Ubrig, N.; Morpurgo, A. F. J. N. 1., Ambipolar light-emitting transistors on chemical vapor deposited monolayer MoS₂. **2015**, *15* (12), 8289-8294.
3. Wang, X.; Chen, Y.; Zheng, B.; Qi, F.; He, J.; Li, Q.; Li, P.; Zhang, W. J. J. o. A.; Compounds, Graphene-like WSe₂ nanosheets for efficient and stable hydrogen evolution. **2017**, *691*, 698-704.
4. Xie, L. J. N., Two-dimensional transition metal dichalcogenide alloys: preparation, characterization and applications. **2015**, *7* (44), 18392-18401.
5. Feng, Q.; Mao, N.; Wu, J.; Xu, H.; Wang, C.; Zhang, J.; Xie, L. J. A. n., Growth of MoS₂ (1-x) Se_{2x} (x= 0.41-1.00) Monolayer Alloys with Controlled Morphology by Physical Vapor Deposition. **2015**, *9* (7), 7450-7455.
6. Mann, J.; Ma, Q.; Odenthal, P. M.; Isarraraz, M.; Le, D.; Preciado, E.; Barroso, D.; Yamaguchi, K.; von Son Palacio, G.; Nguyen, A. J. A. M., 2-Dimensional transition metal dichalcogenides with tunable direct band gaps: MoS₂ (1-x) Se_{2x} monolayers. **2014**, *26* (9), 1399-1404.
7. Li, H.; Duan, X.; Wu, X.; Zhuang, X.; Zhou, H.; Zhang, Q.; Zhu, X.; Hu, W.; Ren, P.; Guo, P. J. J. o. t. A. C. S., Growth of alloy MoS₂ x Se₂ (1-x) nanosheets with fully tunable chemical compositions and optical properties. **2014**, *136* (10), 3756-3759.
8. Feng, Q.; Zhu, Y.; Hong, J.; Zhang, M.; Duan, W.; Mao, N.; Wu, J.; Xu, H.; Dong, F.; Lin, F. J. A. M., Growth of large-area 2D MoS₂ (1-x) Se_{2x} semiconductor alloys. **2014**, *26* (17), 2648-2653.
9. Chen, Y.; Dumcenco, D. O.; Zhu, Y.; Zhang, X.; Mao, N.; Feng, Q.; Zhang, M.; Zhang, J.; Tan, P.-H.; Huang, Y.-S. J. N., Composition-dependent Raman modes of Mo_{1-x}W_xS₂ monolayer alloys. **2014**, *6* (5), 2833-2839.
10. Song, J.-G.; Ryu, G. H.; Lee, S. J.; Sim, S.; Lee, C. W.; Choi, T.; Jung, H.; Kim, Y.; Lee, Z.; Myoung, J.-M. J. N. c., Controllable synthesis of molybdenum tungsten disulfide alloy for vertically composition-controlled multilayer. **2015**, *6*, 7817.
11. Zhang, M.; Wu, J.; Zhu, Y.; Dumcenco, D. O.; Hong, J.; Mao, N.; Deng, S.; Chen, Y.; Yang, Y.; Jin, C. J. A. n., Two-dimensional molybdenum tungsten diselenide alloys: photoluminescence, Raman scattering, and electrical transport. **2014**, *8* (7), 7130-7137.
12. Fu, Q.; Yang, L.; Wang, W.; Han, A.; Huang, J.; Du, P.; Fan, Z.; Zhang, J.; Xiang, B. J. A. M., Synthesis and enhanced electrochemical catalytic performance of monolayer WS₂ (1-x) Se_{2x} with a tunable band gap. **2015**, *27* (32), 4732-4738.
13. Wu, X.; Li, H.; Liu, H.; Zhuang, X.; Wang, X.; Fan, X.; Duan, X.; Zhu, X.; Zhang, Q.; Meixner, A. J. J. N., Spatially composition-modulated two-dimensional WS₂ x Se₂ (1-x) nanosheets. **2017**, *9* (14), 4707-4712.
14. Empante, T. A.; Zhou, Y.; Klee, V.; Nguyen, A. E.; Lu, I.-H.; Valentin, M. D.; Naghibi Al Villar, S. A.; Preciado, E.; Berges, A. J.; Merida, C. S. J. A. n., Chemical vapor deposition growth of few-layer MoTe₂ in the 2H, 1T', and 1T phases: tunable properties of MoTe₂ films. **2017**, *11* (1), 900-905.
15. Oliver, S. M.; Beams, R.; Krylyuk, S.; Kalish, I.; Singh, A. K.; Bruma, A.;

- Tavazza, F.; Joshi, J.; Stone, I. R.; Stranick, S. J.; Davydov, A. V.; Vora, P. M., The structural phases and vibrational properties of $\text{Mo}_{1-x}\text{W}_x\text{Te}_2$ alloys. *2D Materials* **2017**, *4* (4), 045008.
16. Lin, J.; Zhou, J.; Zuluaga, S.; Yu, P.; Gu, M.; Liu, Z.; Pantelides, S. T.; Suenaga, K. J. A. n., Anisotropic Ordering in 1T' Molybdenum and Tungsten Ditelluride Layers Alloyed with Sulfur and Selenium. **2018**, *12* (1), 894-901.
17. Apte, A.; Krishnamoorthy, A.; Hachtel, J. A.; Susarla, S.; Idrobo, J. C.; Nakano, A.; Kalia, R. K.; Vashishta, P.; Tiwary, C. S.; Ajayan, P. M. J. C. o. M., Telluride-Based Atomically Thin Layers of Ternary Two-Dimensional Transition Metal Dichalcogenide Alloys. **2018**, *30* (20), 7262-7268.
18. Li, S.; Wang, S.; Tang, D.-M.; Zhao, W.; Xu, H.; Chu, L.; Bando, Y.; Golberg, D.; Eda, G. J. A. M. T., Halide-assisted atmospheric pressure growth of large WSe_2 and WS_2 monolayer crystals. **2015**, *1* (1), 60-66.
19. Zhou, J.; Lin, J.; Huang, X.; Zhou, Y.; Chen, Y.; Xia, J.; Wang, H.; Xie, Y.; Yu, H.; Lei, J. J. N., A library of atomically thin metal chalcogenides. **2018**, *556* (7701), 355.
20. Yu, P.; Lin, J.; Sun, L.; Le, Q. L.; Yu, X.; Gao, G.; Hsu, C. H.; Wu, D.; Chang, T. R.; Zeng, Q. J. A. M., Metal–Semiconductor Phase-Transition in WSe_2 (1-x) Te_2x Monolayer. **2017**, *29* (4), 1603991.
21. Mahjouri-Samani, M.; Liang, L.; Oyedele, A.; Kim, Y.-S.; Tian, M.; Cross, N.; Wang, K.; Lin, M.-W.; Boulesbaa, A.; Rouleau, C. M. J. N. l., Tailoring vacancies far beyond intrinsic levels changes the carrier type and optical response in monolayer MoSe_2-x crystals. **2016**, *16* (8), 5213-5220.
22. Mignuzzi, S.; Pollard, A. J.; Bonini, N.; Brennan, B.; Gilmore, I. S.; Pimenta, M. A.; Richards, D.; Roy, D. J. P. R. B., Effect of disorder on Raman scattering of single-layer MoS_2 . **2015**, *91* (19), 195411.
23. Shi, W.; Lin, M.-L.; Tan, Q.-H.; Qiao, X.-F.; Zhang, J.; Tan, P.-H. J. D. M., Raman and photoluminescence spectra of two-dimensional nanocrystallites of monolayer WS_2 and WSe_2 . **2016**, *3* (2), 025016.

Supporting Information

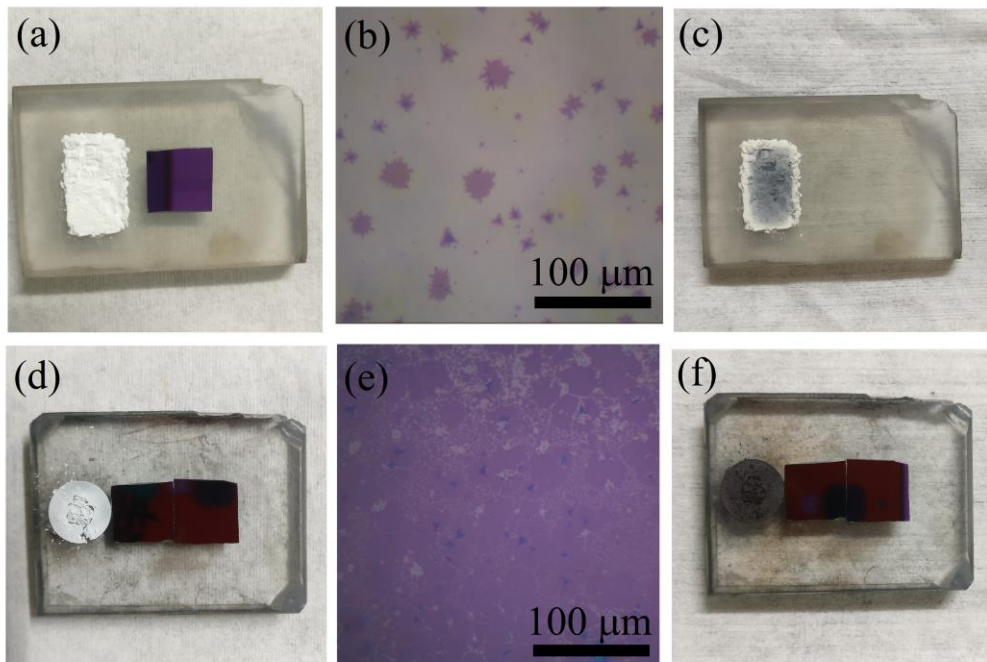


Figure S1 Comparisons of the traditional NaCl assisted CVD method and our modified NaCl assisted CVD method

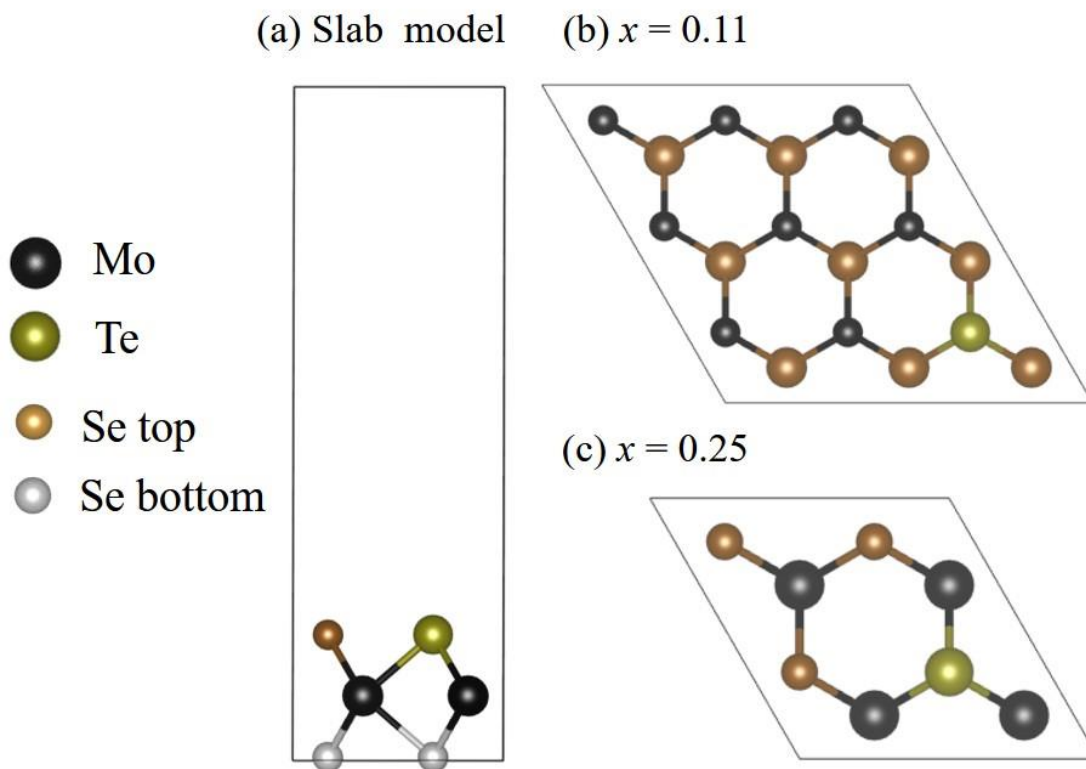


Figure S2 Slab models of 2D $\text{MoTe}_x\text{Se}_{2-x}$ used in our DFT calculation